

# Variational Auto-Regressive Gaussian Processes for Continual Learning

Sanyam Kapoor<sup>1</sup> Theofanis Karaletsos<sup>2</sup> Thang D. Bui<sup>3</sup>

## Abstract

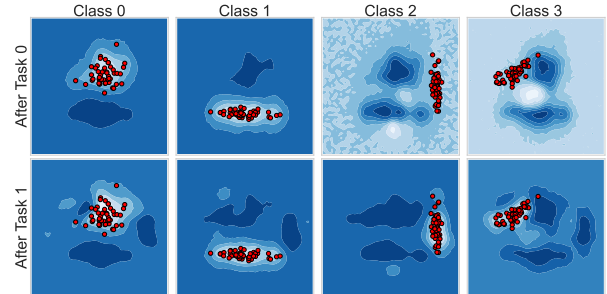
Through sequential construction of posteriors on observing data online, Bayes’ theorem provides a natural framework for continual learning. We develop *Variational Auto-Regressive Gaussian Processes* (VAR-GPs), a principled posterior updating mechanism to solve sequential tasks in continual learning. By relying on sparse inducing point approximations for scalable posteriors, we propose a novel auto-regressive variational distribution which reveals two fruitful connections to existing results in Bayesian inference, expectation propagation and orthogonal inducing points. Mean predictive entropy estimates show VAR-GPs prevent catastrophic forgetting, which is empirically supported by strong performance on modern continual learning benchmarks against competitive baselines. A thorough ablation study demonstrates the efficacy of our modeling choices.

## 1. Introduction

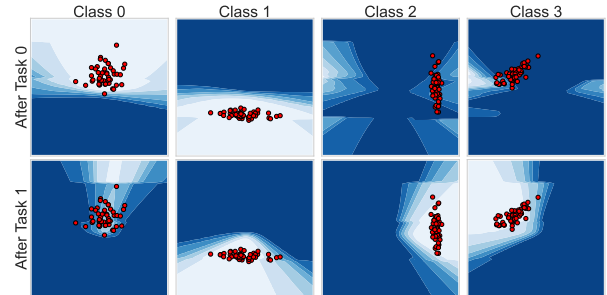
Continual Learning (CL) is the constant development of complex behaviors by building upon previously acquired skills (Ring, 1994; Thrun, 1998); humans and other animals exhibit knowledge acquisition for continual skill development (Hoppitt & Laland, 2013). To the contrary, modern artificial intelligence methods based on supervised machine learning rely on a stronger assumption of all representative information being available at once, i.e. *i.i.d* data. Many systems, however, violate this assumption. A hospital may not have legal access to past patient data to provide automated diagnosis, real-time learning systems may be limited by compute to utilize all available data, and a mobile device may prefer on-device learning and inference to guarantee user privacy. In each of these examples, the learning algo-

Work done when the authors were at Uber AI, San Francisco, CA, USA. <sup>1</sup>Center for Data Science, New York University, New York, NY, USA <sup>2</sup>Facebook Inc., Menlo Park, CA, USA <sup>3</sup>University of Sydney, Sydney, NSW, Australia. Correspondence to: Sanyam Kapoor <sanyam@nyu.edu>.

*Proceedings of the 38<sup>th</sup> International Conference on Machine Learning*, PMLR 139, 2021. Copyright 2021 by the author(s).



(a) VAR-GP (ours)



(b) VCL (with coreset size 10)

Figure 1. By first, only training on classes 0/1 (**Task 0**), and next, only training on classes 2/3 (**Task 1**), we show the posterior predictive density surface (brighter is higher) for a four-way classifier on the synthetic dataset (marked ●) from Figure 2. (a) VAR-GPs preserve information from Task 0 even after training on Task 1, i.e. prevent *catastrophic forgetting* (seen as bright regions around data from Task 0). (b) VCL is overconfident in its predictions and is structurally less stable (seen as large variations in predictive probabilities between Task 0 and Task 1).

gorithm does not observe *i.i.d* data, but only new parts of the data space. We still want to improve our models using new data without compromising existing performance.

Conventional training methods, however, tend to perform poorly when it comes to balancing *rigidity*: the inability to adapt to new experience, and *plasticity*: the tendency to forget past experience. For example, neural network training is known to be vulnerable to *catastrophic forgetting*, causing any data distribution shift to override past learning (McCloskey & Cohen, 1989; Ratcliff, 1990). Many approaches have been pursued to address these issues, and among them, the Bayesian framework is arguably the most

general and principled. By allowing us to sequentially construct posteriors after observing data online, Bayes’ theorem provides a coherent framework to build continual learning algorithms, and avoid pitfalls like catastrophic forgetting; this principle is seen in Sato (2001) for online model selection, and in Broderick et al. (2013) for inference on streaming data. More recently, much literature has been devoted to scalable posterior updating schemes with neural networks — regularization using a Laplace approximation with a diagonal Fisher information matrix (Kirkpatrick et al., 2017), using approximate path integral of gradient vector fields (Zenke et al., 2017), using recursive variational posterior approximations (Nguyen et al., 2018; Swaroop et al., 2019; Ahn et al., 2019), targeting adaptive capacity in Bayesian neural networks (Kessler et al., 2019), and using episodic memory (Lopez-Paz & Ranzato, 2017; Rebuffi et al., 2017). Alternatively, the effectiveness of Gaussian Process (GP) priors is demonstrated by Csátó & Opper (2002) for online regression, and by Bui et al. (2017a) for streaming data. Despite favorable properties, GPs remain under-explored for modern continual learning tasks.

We take a step in this direction and propose *Variational Auto-Regressive Gaussian Processes* (VAR-GPs) for continual learning. By utilizing scalable sparse approximations for Gaussian processes (Titsias, 2009; Hensman et al., 2013; 2015) and advances in variational inference (Hoffman et al., 2013), we make the following key contributions — i) a generalized continual variational lower bound for sequential datasets with a natural interpretation, ii) a novel auto-regressive variational distribution for continual learning with GPs, iii) two fruitful connections to results in Bayesian inference, Expectation Propagation (EP) and orthogonal inducing point approximation, and iv) evidence on the effectiveness of hyper-priors.

The rest of the paper is organized as follows — Section 2 puts prior work in context and highlights the key similarities or differences. Section 3 summarizes the relevant background needed to develop VAR-GPs. Section 4 derives VAR-GPs for continual learning and describes connections to two existing results in Bayesian inference. Section 5 develops an intuitive characterization of how VAR-GPs avoid catastrophic forgetting, supported by empirical results and thorough ablation studies. Finally, Section 6 concludes with a discussion on limitations and future directions.

## 2. Related Work

Our work aligns with the key desiderata for continual learning outlined by Farquhar & Gal (2018) and van de Ven & Tolias (2019). In particular, unlike prior work (Kirkpatrick et al., 2017; Zenke et al., 2017; Nguyen et al., 2018; Swaroop et al., 2019) where task identity is revealed by

a multi-head architecture, we tackle a considerably harder and more realistic continual learning setup where task identity is unknown and rely on approximate Bayesian inference for all learning. While the broader literature focuses on many aspects of CL like vanilla transfer learning (Li & Hoiem, 2017), adaptive model capacity, and episodic memory, we emphasize on developing an automated posterior updating mechanism for continual learning.

Continual learning with neural networks relies on regularization of the parameters through the previous approximate posterior (or the prior in absence of learning) - *Elastic Weight Consolidation* (EWC) (Kirkpatrick et al., 2017) uses Laplace approximations with a diagonal Fisher Matrix, *Synaptic Intelligence* (SI) (Zenke et al., 2017) uses approximate path integral of gradient vector fields, and *RWalk* (Chaudhry et al., 2018) unifies these methods from a KL-divergence perspective. Ritter et al. (2018) use Kronecker-factored approximated Laplace approximation for tractability instead. By directly estimating a recursive approximate variational posterior, *Improved Variational Continual Learning* (VCL) (Nguyen et al., 2018; Swaroop et al., 2019) proves to be one of the most competitive methods, and forms our main baseline. Although, in principle VCL relies on regularizing only w.r.t the last constructed posterior, in practice episodic memory (Swaroop et al., 2019; Shin et al., 2017; Rebuffi et al., 2017) of real samples is used to limit catastrophic forgetting. We avoid this ad-hoc data subset selection problem by naturally incorporating past tasks into our learning objective.

Model capacity has been investigated by *Progressive Neural Networks* (Rusu et al., 2016; Schwarz et al., 2018), which adapt by rewiring neural networks. Kessler et al. (2019) provide a fully Bayesian treatment through Indian Buffet Process priors. While, assessing model capacity required for both batch and continual learning remains an open problem, including in GP-based models, we emphasize only on an automated inference scheme in this work.

Csátó & Opper (2002); Csátó (2002) are seminal contributions towards utilizing Gaussian processes (GPs) in online regression. In the spirit of streaming variational Bayes framework (Broderick et al., 2013), Bui et al. (2017a) demonstrate the effectiveness of GPs for a single-task online regression problems. Moreno-Muñoz et al. (2019) adapt recursive construction from VCL (Nguyen et al., 2018) to multi-task GPs. To the best of our knowledge, no prior work addresses modern continual learning benchmarks and desiderata with GPs alone. More recently, FCRL (Titsias et al., 2020) applies functional regularization to neural networks using sparse GPs, unifying memory-based (Lopez-Paz & Ranzato, 2017; Rebuffi et al., 2017) and Bayesian methods through inducing points selection. Unlike FCRL, our proposed approach naturally

models cross-task covariances through structured approximations, and allows joint optimization of both the variational approximation and inducing inputs using a unified objective.

### 3. Background

**Exact Gaussian processes** We assume basic familiarity with Gaussian processes (GPs) (Rasmussen & Williams, 2005). By expressing priors over the function space, GPs provide a flexible non-parametric framework to perform probabilistic inference. For a dataset  $\mathcal{D}$  of size  $N$ , we model the relationship between a collection of inputs  $\mathbf{X} = \{\mathbf{x}_i\}_{i=1}^N$  and targets  $\mathbf{y} = \{y_i\}_{i=1}^N$  using a Gaussian Process prior  $f | \theta \sim \mathcal{GP}(\mu_\theta(\cdot), k_\theta(\cdot, \cdot))$  and a likelihood model  $p(\mathbf{y} | f(\mathbf{X}))$ . The prior is fully defined by a mean function  $\mu_\theta$  and a covariance function  $k_\theta$ , where  $\theta$  is a small set of hyperparameters. Often, we will denote the covariance matrix as  $\mathbf{K}_{\mathbf{X}, \mathbf{Z}}$  to be explicit about the two sets of inputs  $\mathbf{X}$  and  $\mathbf{Z}$  that generate the matrix, keeping dependence on  $\theta$  implicit. As typical in literature, we set the mean function to zero.

The intertwined goals of exact inference are to infer the posterior distribution  $p(f | \mathcal{D}, \theta)$  and obtain the marginal likelihood  $p(\mathbf{y} | \mathbf{X}, \theta) = \int p(\mathbf{y} | f(\mathbf{X}))p(f | \theta)df$ . The posterior distribution can be used to obtain the predictive distribution for a novel input  $\mathbf{x}_*$ , as  $p(\mathbf{y}_* | \mathbf{x}_*, \mathcal{D}, \theta) = \int p(\mathbf{y}_* | f(\mathbf{x}_*))p(f | \mathcal{D}, \theta)df$ , while the marginal likelihood can be used for model selection. For instance, a Gaussian likelihood model with a diagonal covariance  $p(\mathbf{y} | f, \mathbf{X}) = \mathcal{N}(\mathbf{y}; f(\mathbf{X}), \sigma_y^2 \mathbf{I})$  leads to closed-form expressions for predictive distribution, which is a Gaussian defined by the following mean and variance,

$$\mu_* = \mathbf{K}_*^T (\mathbf{K} + \sigma_y^2 \mathbf{I})^{-1} \mathbf{y}, \quad (1)$$

$$\sigma_*^2 = \mathbf{K}_{**} - \mathbf{K}_*^T (\mathbf{K} + \sigma_y^2 \mathbf{I})^{-1} \mathbf{K}_*, \quad (2)$$

where  $\mathbf{K}_{**} = k_\theta(\mathbf{x}_*, \mathbf{x}_*)$ , and the covariance matrices are given by  $(\mathbf{K}_*)_i = k_\theta(\mathbf{x}_i, \mathbf{x}_*)$ , and  $(\mathbf{K})_{ij} = k_\theta(\mathbf{x}_i, \mathbf{x}_j)$ . This model can be extended for  $K$ -way classification by building  $K$  independent functions and using a *softmax* likelihood function such that class probabilities are given by  $p(y = k | f_1, \dots, f_K, \mathbf{x}) \propto \exp\{f_k(\mathbf{x})\}$ .

Unfortunately, exact inference is analytically and computationally intractable for many models and datasets of interest. Even for the closed-form solution above for GP regression, the computational complexity is  $\mathcal{O}(N^3)$  for inference & learning, and  $\mathcal{O}(N^2)$  for every subsequent prediction. We will rely on sparse variational approximations to sidestep both intractabilities.

**Sparse Variational Gaussian processes** Among various sparse approximations of Gaussian processes (Quiñero-

Candela & Rasmussen, 2005; Bui et al., 2017b), our continual learning algorithm builds on inducing-point methods (Titsias, 2009; Hensman et al., 2013; 2015). Following Hensman et al. (2015), we introduce  $M$  inducing outputs  $\mathbf{u} = \{u_i\}_{i=1}^M$ , and corresponding inducing inputs  $\mathbf{Z} = \{\mathbf{z}_i\}_{i=1}^M$ . We view  $\mathbf{u}, \mathbf{Z}$  not simply as a collection of points, but  $\mathbf{u}$  as values of a continuous function  $f$  evaluated at  $\mathbf{Z}$ , i.e.  $\mathbf{u} = f(\mathbf{Z})$ . By noting that the underlying function can be decomposed as  $f = \{f_{\neq \mathbf{u}}, \mathbf{u}\}$ , the joint distribution can be equivalently written as,

$$p(\mathbf{y}, f | \mathbf{X}, \theta) = p(\mathbf{y} | f, \mathbf{X}) p(f_{\neq \mathbf{u}} | \mathbf{u}, \theta) p(\mathbf{u} | \mathbf{Z}, \theta). \quad (3)$$

The structured variational approximation is judiciously chosen to be  $q(f) = p(f_{\neq \mathbf{u}} | \mathbf{u}, \theta) q(\mathbf{u})$ . This leads to a cancellation of difficult terms, yielding the following variational lower bound,

$$\begin{aligned} \mathcal{F}(q, \theta) &= \mathbb{E}_{q(f)} \left[ \log \frac{p(\mathbf{y} | f) p(f_{\neq \mathbf{u}} | \mathbf{u}, \theta) p(\mathbf{u} | \mathbf{Z}, \theta)}{p(f_{\neq \mathbf{u}} | \mathbf{u}, \theta) q(\mathbf{u})} \right] \\ \mathcal{F}(q, \theta) &= \sum_{i=1}^N \mathbb{E}_{q(f)} [\log p(y_i | f, \mathbf{x}_i)] \\ &\quad - \mathcal{KL}[q(\mathbf{u}) || p(\mathbf{u} | \theta)]. \end{aligned} \quad (4)$$

The first term in this bound remains intractable for a general likelihood and large  $N$ . However, it can be approximated by simple Monte Carlo with reparameterisation gradients and data subsampling (Jordan et al., 1999; Hoffman et al., 2013; Hensman et al., 2013). Bui et al. (2017a) extend this bound for streaming data, and show good performance on time series regression. This approach, however, employs a single set of inducing points which is *shared* across multiple time steps or tasks and, as a result, the inducing points are either too rigid to adapt, or too quickly moving to regions of new data. We demonstrate this pitfall in Section 5. Equipped with this background, we are now ready to derive the proposed approximation, VAR-GPs.

## 4. Variational Auto-Regressive Gaussian Processes

Consider datasets  $\{\mathcal{D}^{(1)}, \dots, \mathcal{D}^{(T)}\}$ , of sizes  $\{N_1, \dots, N_T\}$  respectively, for  $T$  different but related tasks. These tasks are observed sequentially and only once. We want a model which performs well not only on the current task, but also sustains performance on previous tasks. In subsequent notations, we identify task-specific quantities with corresponding task numbers,  $\{1, \dots, T\}$ .

### 4.1. Learning the First Task

We first extend the model in (3) to incorporate a prior over the hyperparameters  $p(\theta)$  and

choose the corresponding variational posterior  $q_1(f, \theta) = p(f_{\neq \mathbf{u}_1} | \mathbf{u}_1, \theta) q(\mathbf{u}_1 | \theta)$ . While the correlation between  $\mathbf{u}$  and  $\theta$  is ignored in the approximate posterior, the dependencies between  $\theta$  and the remaining function values are retained through the conditional prior term. Learning the first task using  $\mathcal{D}^{(1)}$  is thus a direct extension of the sparse variational approach in Section 3, leading to the following bound,

$$\begin{aligned} \mathcal{F}(q_1) = & \sum_{i=1}^{N_1} \mathbb{E}_{q_1(f, \theta)} \left[ \log p \left( y_i^{(1)} | f, \mathbf{x}_i^{(1)} \right) \right] \\ & - \mathcal{KL} [q_1(\theta) || p(\theta)] \\ & - \mathbb{E}_{q_1(\theta)} [\mathcal{KL} [q(\mathbf{u}_1) || p(\mathbf{u}_1 | \theta)]] . \end{aligned} \quad (5)$$

We stress that quantifying uncertainty in hyperparameters through  $q_1(\theta)$  is important for continual learning, as supported by our ablation studies in Section 5.3.

## 4.2. Generalized Continual Variational Lower Bound

Instead of reusing and updating the same set of inducing inputs and outputs for all subsequent tasks as in Bui et al. (2017a), we introduce a separate set of inducing inputs and outputs,  $\{\mathbf{Z}_t, \mathbf{u}_t\}$ , for each task. Consider the  $t$ -th task and  $t > 1$ , using notation in a spirit similar to (3), the function can be split into,  $f = \{f_{\neq \mathbf{u}_{\leq t}}, \mathbf{u}_{\leq t}, \mathbf{u}_t\}$  that describes a decomposition in terms of all past inducing outputs  $\mathbf{u}_{< t}$  and current inducing outputs  $\mathbf{u}_t$ . This leads to an approximate running joint for  $\mathcal{D}^{(t)}$  conditioned on past data as,

$$\begin{aligned} p(\mathbf{y}^{(t)}, f, \theta | \mathbf{X}^{(t)}, \mathcal{D}^{(<t)}) \approx & \prod_{i=1}^{N_t} p(y_i^{(t)} | f, \mathbf{x}_i^{(t)}) \\ & p(f_{\neq \mathbf{u}_{\leq t}} | \mathbf{u}_{\leq t}, \theta) \\ & p(\mathbf{u}_t | \mathbf{Z}_t, \mathbf{u}_{< t}, \theta) \\ & q(\mathbf{u}_{< t} | \mathbf{Z}_{< t}, \theta) \\ & q_{t-1}(\theta) . \end{aligned} \quad (6)$$

We mirror the form of the prior in the approximate posterior, in a similar fashion to the first task, to obtain the following variational distribution,

$$\begin{aligned} q_t(f, \theta) = & p(f_{\neq \mathbf{u}_{\leq t}} | \mathbf{u}_{\leq t}, \theta) q(\mathbf{u}_t | \mathbf{Z}_t, \mathbf{u}_{< t}, \mathbf{Z}_{< t}, \theta) \\ & q(\mathbf{u}_{< t} | \mathbf{Z}_{< t}, \theta) q_t(\theta) . \end{aligned} \quad (7)$$

This structured form leads to the cancellation of  $p(f_{\neq \mathbf{u}_{\leq t}} | \mathbf{u}_{\leq t}, \theta)$  and  $q(\mathbf{u}_{< t} | \mathbf{Z}_{< t}, \theta)$  to arrive at the generalized continual variational lower bound,

$$\begin{aligned} \mathcal{F}(q_t) = & \sum_{i=1}^{N_t} \mathbb{E}_{q_t(f, \theta)} \left[ \log p(y_i^{(t)} | f, \mathbf{x}_i^{(t)}) \right] \\ & - \mathcal{KL} [q_t(\theta) || q_{t-1}(\theta)] \\ & - \mathbb{E}_{q_t(\theta) q(\mathbf{u}_{< t} | \mathbf{Z}_{< t}, \theta)} [\mathfrak{D}_t] , \end{aligned} \quad (8)$$

where,

$$\mathfrak{D}_t = \mathcal{KL} [q(\mathbf{u}_t | \mathbf{Z}_t, \mathbf{u}_{< t}, \mathbf{Z}_{< t}, \theta) || p(\mathbf{u}_t | \mathbf{Z}_t, \mathbf{u}_{< t}, \mathbf{Z}_{< t}, \theta)] .$$

We emphasize that any dependence on  $\mathbf{u}_t$  is accompanied by corresponding  $\mathbf{Z}_t$  as presented in (1) and (2), but may often keep it implicit for concise notation.

As our learning objective, the maximization of (8) takes a natural interpretation — we maximize the likelihood of current data  $\mathcal{D}^{(t)}$ , subject to a  $\mathcal{KL}$ -regularization that balances past posterior and new data. The regularization term involves hyperparameters and current inducing outputs. In practice, tempering the hyperparameter distribution may prove helpful under misspecified models (Wenzel et al., 2020; Wilson & Izmailov, 2020), which is equivalent to scaling  $\mathcal{KL} [q_t(\theta) || q_{t-1}(\theta)]$  by a positive scalar  $\beta$ . The new inducing points  $\{\mathbf{Z}_t, \mathbf{u}_t\}$  are used to explain new parts of the data space while the old ones  $\{\mathbf{Z}_{< t}, \mathbf{u}_{< t}\}$  aim to preserve past experience, as demonstrated in Figure 1. Next, we develop this intuition further, and experimentally demonstrate in Section 5.1.

## 4.3. Distributional Choices

We now detail the parametrizations for all aforementioned distributions. All prior-related densities, i.e.  $p(\mathbf{u}_1 | \theta)$ ,  $p(\mathbf{u}_t | \mathbf{u}_{< t}, \theta)$ , and  $p(f_{\mathbf{u}_{\leq t}} | \mathbf{X}^{(t)}, \mathbf{u}_{\leq t}, \theta)$  can be computed by invoking the GP prior. All experiments use the Exponentiated Quadratic kernel such that  $\theta$  includes the log-ARD lengthscales and a log-scale factor (see Appendix C.1). The prior over the log-hyperparameters for the first task  $p(\theta)$  is assumed to be a standard Normal,  $\mathcal{N}(\theta; \mathbf{0}, \mathbf{I})$ .

The variational distribution of the log-hyperparameters is assumed to be a mean-field Gaussian, i.e. parametrized by a diagonal covariance,  $q_t(\theta) = \mathcal{N}(\theta; \boldsymbol{\mu}_t, \text{diag}(\boldsymbol{\sigma}_t))$ . These choices allow for closed-form  $\mathcal{KL}$  computations in (5) and (8). The variational distribution over inducing outputs for the first task is parametrized as  $q(\mathbf{u}_1) = \mathcal{N}(\mathbf{u}_1; \mathbf{m}_1, \boldsymbol{\Sigma}_1)$  for a set of  $M_1$  inducing outputs, as standard in sparse variational GPs using mean  $\mathbf{m}_1$  and covariance matrix  $\boldsymbol{\Sigma}_1$ .

One of our key contributions is an auto-regressive parametrization for the variational distribution given by  $q(\mathbf{u}_{\leq t} | \theta) = q(\mathbf{u}_1) \prod_{j=2}^t q(\mathbf{u}_j | \mathbf{u}_{< j}, \theta)$ , where  $q(\mathbf{u}_t | \mathbf{u}_{< t}, \theta) = \mathcal{N}(\mathbf{u}_t; \mathbf{K}_{\mathbf{Z}_t, \mathbf{Z}_{< t}} \mathbf{K}_{\mathbf{Z}_{< t}, \mathbf{Z}_{< t}}^{-1} \mathbf{u}_{< t} + \mathbf{m}_t, \boldsymbol{\Sigma}_t)$  relies on  $M_t$  inducing variables for all subsequent tasks  $t > 1$ . As a consequence of this structure,  $\mathfrak{D}_t$  becomes independent of  $\mathbf{u}_{< t}$  and avoids sampling variance introduced by samples from  $q(\mathbf{u}_{< t} | \mathbf{Z}_{< t}, \theta)$ . A simplifying trick to compute  $q(\mathbf{u}_{< t} | \theta)$  using conditional Gaussian identities (see Appendix C.3). We further note that (i) the marginal density for inducing outputs  $\mathbf{u}_t$  when  $t > 1$  is non-Gaussian, and (ii) even though  $\mathbf{Z}_t, \mathbf{m}_t, \boldsymbol{\Sigma}_t$  are kept

fixed after training on the  $t$ -th task, the marginal density  $q(\mathbf{u}_t)$  can still change over time due to the change in  $q(\theta)$ .

Next, Sections 4.3.1 and 4.3.2 provide two fruitful connections of the proposed structured variational approximation to existing literature.

#### 4.3.1. STRUCTURED EP FACTOR APPROXIMATION LEADS TO AN AUTO-REGRESSIVE APPROXIMATE POSTERIOR

For the approximate running joint in (6), we can introduce an approximation to the posterior as,

$$q_t(f, \theta) \propto \left[ \prod_{i=1}^{N_t} \mathbf{g}_i^{(t)}(\theta) \mathbf{h}_i^{(t)}(\mathbf{u}_t) \right] p(f_{\neq \mathbf{u}_{\leq t}} | \mathbf{u}_{\leq t}, \theta) \quad (9)$$

$$q(\mathbf{u}_{< t} | \theta) p(\mathbf{u}_t | \mathbf{u}_{< t}, \theta) q_{t-1}(\theta),$$

where the difficult likelihood term,  $\prod_{i=1}^{N_t} p(y_i^{(t)} | f, \mathbf{x}_i^{(t)})$ , is approximated by  $\prod_{i=1}^{N_t} \mathbf{g}_i^{(t)}(\theta) \mathbf{h}_i^{(t)}(\mathbf{u}_t)$  such that  $\mathbf{g}_i$  and  $\mathbf{h}_i$  are the approximate contributions of each likelihood term to the posterior. Expectation Propagation (EP) (Minka, 2001) then proceeds by repeating the following steps to convergence: i) remove the approximate contributions  $\mathbf{g}_i$  and  $\mathbf{h}_i$  from the posterior to form the cavity for  $i$ -th datum, ii) merge the cavity with  $p(y_i^{(t)} | f, \mathbf{x}_i^{(t)})$  to form the tilted distribution  $\tilde{p}_i$ , iii) minimize the divergence  $\mathcal{KL}[\tilde{p}_i || q_t]$  to find a new approximate posterior, and iv) obtain the new approximate factors  $\mathbf{g}_i$  and  $\mathbf{h}_i$  by removing the cavity from the new posterior.

We are, however, not interested in running EP, but only in the form of the approximate posterior induced by EP. Merging relevant terms in the approximate posterior as

$$q_t(f, \theta) \propto p(f_{\neq \mathbf{u}_{\leq t}} | \mathbf{u}_{\leq t}, \theta)$$

$$q(\mathbf{u}_t | \mathbf{u}_{< t}, \theta) q(\mathbf{u}_{< t} | \theta) \quad (10)$$

$$q_t(\theta),$$

where,

$$q_t(\theta) \propto q_{t-1}(\theta) \prod_{i=1}^{N_t} \mathbf{g}_i^{(t)}(\theta),$$

$$q(\mathbf{u}_t | \mathbf{u}_{< t}, \theta) \propto p(\mathbf{u}_t | \mathbf{u}_{< t}, \theta) \prod_{i=1}^{N_t} \mathbf{h}_i^{(t)}(\mathbf{u}_t).$$

We find that the auto-regressive factor is given by  $p(\mathbf{u}_t | \mathbf{u}_{< t}, \theta) = \mathcal{N}(\mathbf{u}_t; \mathbf{A}_t \mathbf{u}_{< t}, \mathbf{C}_t)$ , where we define  $\mathbf{A}_t \triangleq \mathbf{K}_{\mathbf{Z}_t, \mathbf{Z}_{< t}} \mathbf{K}_{\mathbf{Z}_{< t}, \mathbf{Z}_{< t}}^{-1}$ , and  $\mathbf{C}_t \triangleq \mathbf{K}_{\mathbf{Z}_t, \mathbf{Z}_t} - \mathbf{K}_{\mathbf{Z}_t, \mathbf{Z}_{< t}} \mathbf{K}_{\mathbf{Z}_{< t}, \mathbf{Z}_{< t}}^{-1} \mathbf{K}_{\mathbf{Z}_{< t}, \mathbf{Z}_t}$ .

Now, consider a Gaussian factor approximation  $\mathbf{H}_t(\mathbf{u}_t) = \prod_{i=1}^{N_t} \mathbf{h}_i(\mathbf{u}_t) = \mathcal{N}(\mathbf{u}_t; \mu, \Sigma)$ . By multiplying  $\mathbf{H}_t(\mathbf{u}_t)$  with  $p(\mathbf{u}_t | \mathbf{u}_{< t}, \theta)$  and renormalizing, we arrive at  $q(\mathbf{u}_t | \mathbf{u}_{< t}, \theta) = \mathcal{N}(\mathbf{u}_t; \tilde{\mu}, \tilde{\Sigma})$ , where

$\tilde{\Sigma}^{-1} = \Sigma^{-1} + \mathbf{C}_t^{-1}$  and  $\tilde{\Sigma}^{-1} \tilde{\mu} = \Sigma^{-1} \mu + \mathbf{C}_t^{-1} \mathbf{A}_t \mathbf{u}_{< t}$ . The conditional posterior mean can be reformulated as  $\tilde{\mu} = \mathbf{A}_t \mathbf{u}_{< t} + (\mathbf{I} + \Sigma \mathbf{C}_t^{-1})^{-1} (\mu - \mathbf{A}_t \mathbf{u}_{< t})$ , so that we can parameterize the conditional posterior instead of the factor  $\mathbf{H}_t(\mathbf{u}_t)$ , giving us  $q(\mathbf{u}_t | \mathbf{u}_{< t}, \theta) = \mathcal{N}(\mathbf{u}_t; \mathbf{A}_t \mathbf{u}_{< t} + \mathbf{m}, \Sigma)$ . This is equivalent to our auto-regressive parametrization.

#### 4.3.2. EQUIVALENCE TO ORTHOGONAL INDUCING POINTS

Our auto-regressive parametrization is also exactly equivalent to the *orthogonal inducing points* formulation when  $T = 2$  (Shi et al., 2020, §3.3). A variational approximation over two set of orthogonal inducing points,  $\mathbf{u}$  and  $\mathbf{v}$ , is presented as

$$q(\mathbf{u}, \mathbf{v}) = \mathcal{N} \left( \begin{bmatrix} \mathbf{u} \\ \mathbf{v} \end{bmatrix}; \begin{bmatrix} \mathbf{m}_u \\ \mathbf{K}_{\mathbf{v}\mathbf{u}} \mathbf{K}_{\mathbf{u}\mathbf{u}}^{-1} \mathbf{m}_u \end{bmatrix}, \Sigma \right), \quad (11)$$

where,

$$\Sigma \triangleq \begin{bmatrix} \Sigma_u & \Sigma_u \mathbf{K}_{\mathbf{u}\mathbf{u}}^{-1} \mathbf{K}_{\mathbf{u}\mathbf{v}} \\ \mathbf{K}_{\mathbf{v}\mathbf{u}} \mathbf{K}_{\mathbf{v}\mathbf{v}}^{-1} \Sigma_u & \Sigma_v + \mathbf{K}_{\mathbf{v}\mathbf{u}} \mathbf{K}_{\mathbf{u}\mathbf{u}}^{-1} \Sigma_u \mathbf{K}_{\mathbf{u}\mathbf{u}}^{-1} \mathbf{K}_{\mathbf{u}\mathbf{v}} \end{bmatrix}.$$

By appealing to conditional Gaussian identities, the joint can be factored as  $q(\mathbf{u}, \mathbf{v}) = q(\mathbf{u})q(\mathbf{v} | \mathbf{u})$ , such that  $q(\mathbf{u}) = \mathcal{N}(\mathbf{u}; \mathbf{m}_u, \Sigma_u)$ , and  $q(\mathbf{v} | \mathbf{u}) = \mathcal{N}(\mathbf{v}; \mathbf{K}_{\mathbf{v}\mathbf{u}} \mathbf{K}_{\mathbf{u}\mathbf{u}}^{-1} \mathbf{u} + \mathbf{m}_v, \Sigma_v)$ . This conditional is exactly equivalent to our proposal when there are two tasks, i.e.  $\mathbf{u} \Leftrightarrow \mathbf{u}_1$  and  $\mathbf{v} \Leftrightarrow \mathbf{u}_2$ . Intuitively, the second set of inducing variables  $\mathbf{u}_2$  attempt to explain the data space that is not well-explained by the first set  $\mathbf{u}_1$ . Shi et al. (2020) briefly discussed using more than two sets of inducing points for a fixed dataset but did not investigate further due to implementation complexity and the potential small gain beyond two sets. Unlike the batch setting of Shi et al. (2020), our work extends the idea of using many sets of such inducing points to the continual learning setting.

## 5. Experiments

Through our experiments, we highlight the qualitative characteristics of the derived generalized learning objective (8), and provide evidence for the competitiveness of VAR-GPs compared to our main baseline Improved Variational Continual Learning (VCL) (Nguyen et al., 2018; Swaroop et al., 2019), among others. A thorough ablation study demonstrates the efficacy of our modeling choices. The full reference implementation of VAR-GPs in PyTorch (Paszke et al., 2019) in publicly available at [u.perhapsbay.es/vargp-code](https://u.perhapsbay.es/vargp-code).

To mimic a real continual learning setting, the model only observes  $\mathcal{D}^{(t)}$  for training and is tested on all the tasks seen

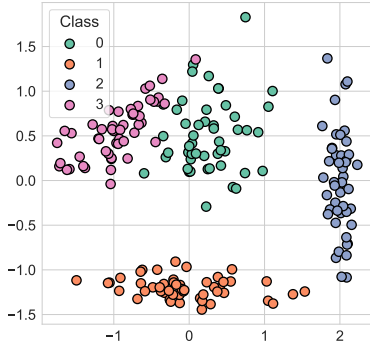


Figure 2. A synthetic toy dataset used for the four-way classification problem in Figure 1.

so far using  $\mathcal{D}^{(\leq t)}$ . We track validation accuracy on a subset of the training set for early stopping. To optimize both variational objectives (5) and (8), we use a mini-batch size of 512 and 3 samples from variational distribution with the Yogi optimizer (Zaheer et al., 2018). Predictive distributions are estimated via 10 Monte-Carlo samples. The training for the  $t$ -th task is summarized in Algorithm 1.

---

#### Algorithm 1 VAR-GP per-task training

---

**Input:** Learning rate  $\eta$ , Batch size  $B$ , Number of inducing points  $M$ , Maximum epochs  $E$ , Task dataset  $\mathcal{D}^{(t)}$ , hyperparameters: KL tempering factor  $\beta$ , Early stopping patience of  $K$  epochs and tolerance  $\delta$

**Output:** Per-task variational approximations for kernel hyper-parameters  $\theta$  and inducing outputs  $\mathbf{u}_t$ , and inducing inputs  $\mathbf{Z}_t$

Initialize  $\mathbf{Z}_t \in \mathbb{R}^{M \times D} \subset \mathbf{X}^{(t)} \in \mathbb{R}^{N_t \times D}$

**for**  $e$  **in**  $1 \dots E$  **do**

**for**  $\{\mathbf{x}_i, y_i\}_{i=1}^B \subset \mathcal{D}^{(t)}$  **do**

    Compute  $\mathcal{F}(q_t)$  — using (5) for the first task, and (8) for all subsequent ones.

    Update  $\theta$ ,  $\mathbf{m}_t$ ,  $\Sigma_t$  and  $\mathbf{Z}_t$  with learning rate  $\eta$  and tempering factor  $\beta$

**end for**

  Compute validation accuracy  $A_e$

**if**  $e > K$  **and**  $|A_e - A_{e-K}| < \delta$  **then**

**break**

**end if**

**end for**

---

All covariance matrices in the variational distributions are modeled as a lower triangular Cholesky factors, described in Appendix C.2, initialized at an identity matrix for numerical stability, with diagonals constrained to be positive during optimization using a `softplus` transform. Further, as described in Appendix C.1, the kernel parameters  $\theta$ , including lengthscales and scale factors modeled as `log`-transforms to maintain positivity. Appendix D.1 lists the

search space for all hyper-parameters. Results report the mean and one standard deviation of five independent trials. Next, we describe the datasets used for experiments.

**Synthetic Classification Dataset** Visualized in Figure 2, we use a synthetic 2-D dataset with four classes in the range  $x, y \in [-3., 3.]$  for qualitative assessments. We observe classes in pairs 0/1 (Task 0) and 2/3 (Task 1), each only once. We do not use any tempering for this dataset, i.e.  $\beta = 1$ .

**Split MNIST** Following Zenke et al. (2017), we consider the full 10-way classification task at each time step but receive a dataset  $\mathcal{D}^{(t)}$  of only a subset of MNIST digits in the sequence 0/1, 2/3, 4/5, 6/7, and 8/9. 10000 training samples are cumulatively set aside for validation set across all tasks. We allocate 60 inducing points for each task, with a learning rate of 0.003, and  $\beta = 10.0$ . We remind the reader that unlike prior work which uses a multi-head model with task information, we only use a single-head to report the classification test accuracy, making the benchmark considerably harder and more representative of reality.

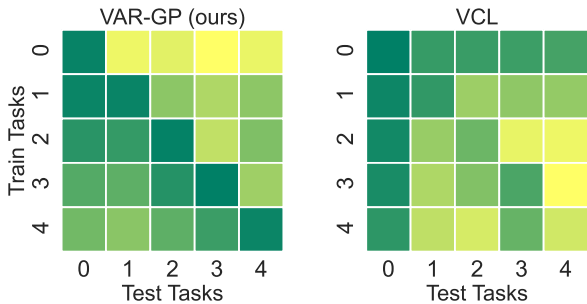
**Permuted MNIST** In this benchmark, we receive a dataset  $\mathcal{D}^{(t)}$  of MNIST digits at each time step  $t$ , such that the pixels undergo an unknown but fixed permutation. 10000 samples are set aside for validation. We allocate 100 inducing points for each task, with a learning rate of 0.0037, and  $\beta = 1.64$ . The first task is fixed to be the unpermuted MNIST to provide an upper bound on the performance of subsequent tasks. While prior work (Zenke et al., 2017; Kirkpatrick et al., 2017) uses this benchmark as an indicator of representational capacity of neural networks, we use this to test performance under distributional shift.

### 5.1. Qualitative Analysis

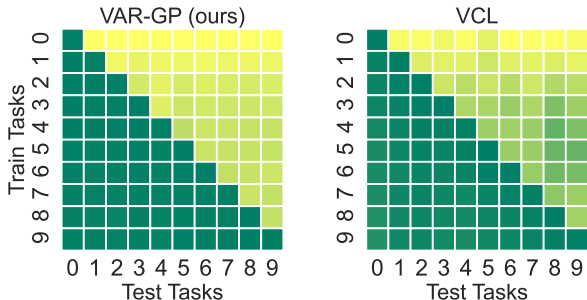
Before presenting benchmark results, we seek to intuitively understand how VAR-GPs learn and avoid *catastrophic forgetting*. By modeling the cross-task covariances through  $\mathcal{Q}_t$  in (8), we are able to bias the learning such that under the given budget of inducing points, VAR-GPs retain information about the previous tasks. This is exemplified in Figure 1. Observing predictive density plots for Classes 0 and 1 after “Task 1”, we notice that the high density regions from “Task 0” are preserved by VAR-GPs, whereas VCL suffers from large variations in the predictions.

This characteristic is not restricted to the toy dataset. Using mean predictive entropy estimates to quantify uncertainty over the test set, we visualize the degree of forgetting for benchmark datasets in Figure 3. Even as tasks progress, VAR-GPs demonstrate information preservation from old tasks by keeping entropy low. In contrast, often being overconfident in predictions, VCL keeps entropy low only for the old tasks at the expense of new ones.





(a) Split MNIST



(b) Permuted MNIST

Figure 3. As we continually train on tasks (shown along the y-axis), we evaluate the mean predictive entropy on the test set for all tasks (shown along the x-axis). In other words, the upper triangular region shows tasks which are not yet seen during training. The values are normalized by the entropy of a random ten-way classifier,  $\log_{10}$ . Brighter regions correspond to a higher entropy, i.e. larger predictive uncertainty. (Top) For Split MNIST, we observe that VAR-GPs lead to lower forgetting rates through lower predictive entropy in the lower triangular regions, and higher uncertainties in upper triangular regions. VCL (Swaroop et al., 2019), on the other hand fails to improve much on subsequent tasks. (Bottom) For Permuted MNIST, we see that while both VAR-GPs and VCL maintain reasonably low catastrophic forgetting on the tasks seen so far, VCL tends to be overconfident on unseen tasks, i.e. low predictive entropy in the upper triangular region.

Finally, an inspection of the optimized inducing points reveals that VAR-GPs tend to focus on covering the regions of the current task, as one would naturally expect. Figure 4 showcases this behavior for Split MNIST. We anticipate such space covering behavior from our learning objective (8) due to the cross-correlations modeled in the regularization term  $\mathcal{D}_t$ .

### 5.2. Benchmark Results

With a qualitative picture of how VAR-GPs learn favorably for sequential tasks in continual learning, we validate its performance on the benchmark datasets of Split MNIST and Permuted MNIST.

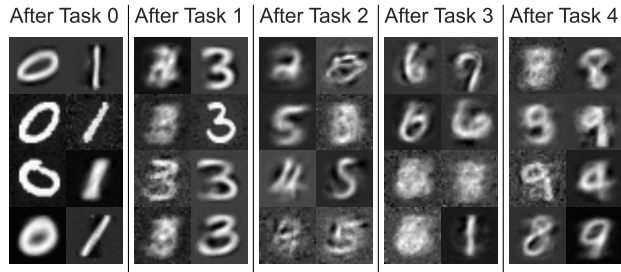
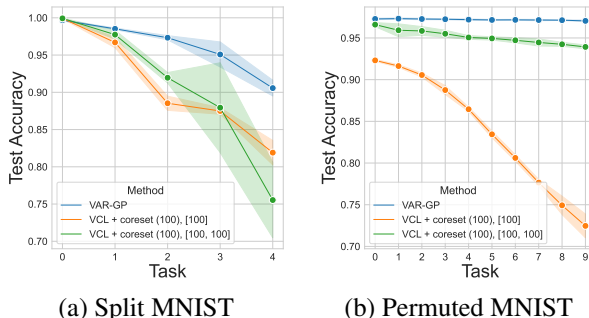


Figure 4. We visualize the inducing points learned after each task in Split MNIST, progressing from left to right. This figure reveals that VAR-GPs spread inducing points to cover the input space for each task.

Figure 5 shows how the cumulative performance across all tasks seen so far evolves as the number of tasks increase. VAR-GPs perform favorably by performing consistently better throughout. One of the most competitive methods, VCL and its variants involving episodic memory through coresets (Swaroop et al., 2019) tend to deteriorate much faster, hinting at catastrophic forgetting. Quantitatively, we find the final mean test accuracy achieved by VAR-GPs after training on five Split MNIST tasks is 90.57%, which is significantly better than the best performing VCL variant at 81.90%. Similarly, VAR-GPs achieve a mean test accuracy of 97.2% after training on ten tasks of Permuted MNIST, as compared to 95.06% by the best variant of VCL. Comparisons against other continual learning algorithms are summarized in Table 1.



(a) Split MNIST

(b) Permuted MNIST

Figure 5. Comparing VAR-GPs to variants of VCL (Nguyen et al., 2018; Swaroop et al., 2019) as we see more tasks (shown along the X-axis). We compute the average test accuracy (show along Y-axis) across all tasks seen so far, including the current one. The plots show mean and one standard deviation across five independent trials. VAR-GPs preserve information from old tasks, avoid catastrophic forgetting and consequently perform much better on newer tasks without compromising on old ones. See Table 1, for all numerical results.

### 5.3. Ablations

Finally, we validate the specific modeling choices in VAR-GPs via a thorough ablation study.

Table 1. The final average test accuracy (in %) after sequential training on benchmark dataset tasks —five for Split MNIST and ten for Permuted MNIST are noted below. We provide the mean and one standard deviation (where available) over five independent trials. \*Split MNIST results for SI (Zenke et al., 2017) and EWC (Kirkpatrick et al., 2017) are taken from VCL (Swaroop et al., 2019), however, are not directly comparable as they use a multi-head setup making evaluation easier; CS = coresets.; [100] and [100, 100] represent hidden layer sizes of the neural networks.

Method	Split MNIST	Permuted MNIST
SI	98.9*	86.02
EWC	63.1*	84.11
VCL, [100]	19.90 ± 0.14	82.94 ± 0.85
+ CS(50)	76.21 ± 2.02	85.80 ± 0.41
+ CS(100)	81.90 ± 1.64	86.45 ± 0.26
VCL, [100, 100]	19.91 ± 7.79	94.31 ± 1.05
+ CS(50)	71.89 ± 5.06	95.43 ± 0.39
+ CS(100)	75.54 ± 1.06	95.06 ± 0.22
VAR-GP (ours)	<b>90.57 ± 1.06</b>	<b>97.20 ± 0.08</b>
+ Block Diag.	78.64 ± 1.41	96.31 ± 0.42
+ MLE Hypers	10.09 ± 0.40	10.07 ± 0.15
+ Global	39.31 ± 0.28	46.02 ± 1.09

### Block-Diagonal Variational Distribution

Instead of the auto-regressive posterior  $q(\mathbf{u}_t | \mathbf{u}_{<t}, \theta) = \mathcal{N}(\mathbf{u}_t; \mathbf{K}_{\mathbf{z}_t, \mathbf{z}_{<t}} \mathbf{K}_{\mathbf{z}_{<t}, \mathbf{z}_{<t}}^{-1} \mathbf{u}_{<t} + \mathbf{m}_t, \Sigma_t)$ , we choose a simpler variational distribution given by  $q'(\mathbf{u}_t | \mathbf{u}_{<t}, \theta) = \mathcal{N}(\mathbf{u}_t; \mathbf{m}_t, \Sigma_t)$ , keeping everything else the same. Effectively, removing the conditioning induces a block diagonal structure in the full covariance matrix across the inducing variables where each block represents the covariance among the inducing points for a given task. This also decouples the inducing points and the hyperparameters in the approximate posterior. We hypothesize that this is detrimental to performance. Figure 6 shows that the long-term continual learning performance tends to deteriorate faster, hinting at *greater* catastrophic forgetting.

**Global Inducing Points** In an alternative model, we completely do away with the auto-regressive nature of the variational distribution and just rely on a single set of inducing points at each time step  $q_t(f, \theta) = q_t(\theta)p(f_{\neq \mathbf{u}_t} | \mathbf{u}_t, \theta)q(\mathbf{u}_t)$ . Bui et al. (2017a) rely on this variational distribution for the inducing points and an MLE estimate of the hyperparameters for streaming regression tasks. See Appendix B.1 for precise modeling details and derivations. The experimental evidence in Figure 6, however, shows that such variational approximation is poor for large scale continual classification tasks.

**MLE Hyperparameters** Quantifying uncertainty about the hyperparameters considerably helps the model to perform well across tasks without a detrimental effect on the old ones. In this section, we validate this hypothesis by simply switching off the  $\mathcal{KL}$ -divergence term for the hyperparameters in both (5) and (8). Instead, we rely on a point estimate of the hyperparameters and use the maximum likelihood estimate at each step. The stark performance comparison is shown in Figure 6. The hyper-parameters are stuck in a local minimum and virtually never recover for subsequent tasks.

**Retraining Old Inducing Points** We also investigate a variant of VAR-GP named Re-VAR-GP where unlike earlier, we retrain the old inducing points  $\mathbf{Z}_{<t}$ . This changes the form of the variational lower bound. The precise details and implications are discussed in Appendix B.2, owing to which we do not pursue this approach further.

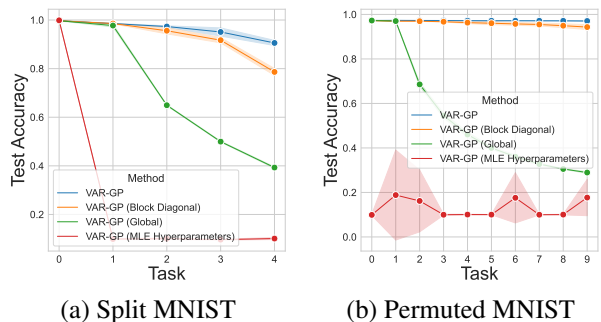


Figure 6. A thorough ablation study reveals the significance of our modeling choices. Evidently, VAR-GPs are able to sustain long-term continual learning performance than any other variant. See Section 5.3 for a detailed description of the ablations conducted.

## 6. Discussion

In this work, we develop VAR-GPs, a principled Bayesian inference scheme for continual learning. Using a sparse inducing point approximation, we propose a structured variational approximation to the true posterior for Gaussian processes, which reveals two fruitful connections to Expectation Propagation and Orthogonal Inducing Points. The resulting lower bound provides a natural learning objective to update the belief over underlying functions as new data arrives. A qualitative characterization of how VAR-GPs learn is presented, backed by strong empirical results on modern continual learning benchmarks. Further, a thorough ablation study establishes the efficacy of modeling choices.

In its current form, the number of inducing points grows linearly in the number of tasks. Consequently, the inference grows cubic in the number of tasks. This computational complexity limits the scaling of VAR-GPs to only a



moderate number of continual learning tasks. Nevertheless, accommodating a post-hoc information distillation procedure in the learning process can prove helpful for scalability, and remains an open research problem. While Gaussian processes provide a flexible approach towards priors in the functional space, the representational power of VAR-GPs can be improved by the use of deep kernel learning. This, however, leads to new regularization challenges to be tackled (see Appendix B.3). Contemporary approaches relying on a memory buffer are also amenable to the proposed inference scheme, since the inducing points provide an automated data selection procedure. Finally, model-based reinforcement learning, where dataset shift is unavoidable, is a promising application space for VAR-GPs.

Through VAR-GPs, we remain optimistic that Gaussian processes provide an effective foundation for predictions under uncertainty in continual learning. More broadly, the characteristics highlighted by our learning objective (8) serve as a principled starting point to guide future research in continual learning objectives.

## Acknowledgements

We would like to thank Matthias Poloczek for insightful conversations along the way. SK was supported by the Uber AI Residency program.

## References

- Ahn, H., Cha, S., Lee, D., and Moon, T. Uncertainty-based continual learning with adaptive regularization. In *Advances in Neural Information Processing Systems*, pp. 4394–4404, 2019. 2
- Broderick, T., Boyd, N., Wibisono, A., Wilson, A. C., and Jordan, M. I. Streaming variational Bayes. In *Advances in Neural Information Processing Systems*, pp. 1727–1735, 2013. 2
- Bui, T. D., Nguyen, C., and Turner, R. E. Streaming sparse Gaussian process approximations. In *Advances in Neural Information Processing Systems*, pp. 3299–3307, 2017a. 2, 3, 4, 8
- Bui, T. D., Yan, J., and Turner, R. E. A unifying framework for Gaussian process pseudo-point approximations using power expectation propagation. *The Journal of Machine Learning Research*, 18(1):3649–3720, 2017b. 3
- Chaudhry, A., Dokania, P. K., Ajanthan, T., and Torr, P. H. Riemannian walk for incremental learning: Understanding forgetting and intransigence. In *Proceedings of the European Conference on Computer Vision*, pp. 532–547, 2018. 2
- Csató, L. *Gaussian processes: iterative sparse approximations*. PhD thesis, Aston University, 2002. 2
- Csató, L. and Opper, M. Sparse on-line Gaussian processes. *Neural computation*, 14(3):641–668, 2002. 2
- Farquhar, S. and Gal, Y. Towards robust evaluations of continual learning. *arXiv preprint arXiv:1805.09733*, 2018. 2
- Hensman, J., Fusi, N., and Lawrence, N. D. Gaussian processes for big data. In *29th Conference on Uncertainty in Artificial Intelligence*, pp. 282–290, 2013. 2, 3
- Hensman, J., Matthews, A. G. D. G., and Ghahramani, Z. Scalable variational Gaussian process classification. In *18th International Conference on Artificial Intelligence and Statistics*, pp. 1–9, 2015. 2, 3
- Hoffman, M. D., Blei, D. M., Wang, C., and Paisley, J. Stochastic variational inference. *The Journal of Machine Learning Research*, 14(1):1303–1347, 2013. 2, 3
- Hoppitt, W. and Laland, K. N. *Social learning: an introduction to mechanisms, methods, and models*. Princeton University Press, 2013. 1
- Jordan, M. I., Ghahramani, Z., Jaakkola, T. S., and Saul, L. K. An introduction to variational methods for graphical models. *Machine learning*, 37(2):183–233, 1999. 3
- Kessler, S., Nguyen, V., Zohren, S., and Roberts, S. Hierarchical Indian buffet neural networks for Bayesian continual learning. *arXiv*, pp. arXiv–1912, 2019. 2
- Kirkpatrick, J., Pascanu, R., Rabinowitz, N., Veness, J., Desjardins, G., Rusu, A. A., Milan, K., Quan, J., Ramalho, T., Grabska-Barwinska, A., et al. Overcoming catastrophic forgetting in neural networks. *Proceedings of the National Academy of Sciences*, 114(13):3521–3526, 2017. 2, 6, 8
- Li, Z. and Hoiem, D. Learning without forgetting. *IEEE transactions on Pattern Analysis and Machine Intelligence*, 40(12):2935–2947, 2017. 2
- Lopez-Paz, D. and Ranzato, M. Gradient episodic memory for continual learning. In *Advances in Neural Information Processing Systems*, pp. 6467–6476, 2017. 2
- McCloskey, M. and Cohen, N. J. Catastrophic interference in connectionist networks: The sequential learning problem. In *Psychology of learning and motivation*, volume 24, pp. 109–165. Elsevier, 1989. 1
- Minka, T. P. Expectation propagation for approximate bayesian inference. In Breese, J. S. and Koller, D. (eds.), *Proceedings of the 17th Conference in Uncertainty in*

- Artificial Intelligence, University of Washington, Seattle, Washington, USA, August 2-5, 2001, pp. 362–369, 2001. 5
- Moreno-Muñoz, P., Artés-Rodríguez, A., and Álvarez, M. A. Continual multi-task Gaussian processes. *arXiv preprint arXiv:1911.00002*, 2019. 2
- Murphy, K. P. *Machine learning: a probabilistic perspective*. MIT press, 2012. 14
- Nguyen, C. V., Li, Y., Bui, T. D., and Turner, R. E. Variational continual learning. In *International Conference on Learning Representations*, 2018. 2, 5, 7
- Paszke, A., Gross, S., Massa, F., Lerer, A., Bradbury, J., Chanan, G., Killeen, T., Lin, Z., Gimelshein, N., Antiga, L., Desmaison, A., Kopf, A., Yang, E., DeVito, Z., Raison, M., Tejani, A., Chilamkurthy, S., Steiner, B., Fang, L., Bai, J., and Chintala, S. Pytorch: An imperative style, high-performance deep learning library. In *Advances in Neural Information Processing Systems 32*, pp. 8024–8035, 2019. 5
- Quiñonero-Candela, J. and Rasmussen, C. E. A unifying view of sparse approximate Gaussian process regression. *Journal of Machine Learning Research*, 6(Dec):1939–1959, 2005. 3
- Rasmussen, C. E. and Williams, C. K. I. *Gaussian Processes for Machine Learning (Adaptive Computation and Machine Learning)*. The MIT Press, 2005. 3
- Ratcliff, R. Connectionist models of recognition memory: constraints imposed by learning and forgetting functions. *Psychological review*, 97(2):285, 1990. 1
- Rebuffi, S.-A., Kolesnikov, A., Sperl, G., and Lampert, C. H. iCaRL: Incremental classifier and representation learning. In *Proceedings of the IEEE conference on Computer Vision and Pattern Recognition*, pp. 2001–2010, 2017. 2
- Ring, M. B. *Continual learning in reinforcement environments*. PhD thesis, University of Texas at Austin, 1994. 1
- Ritter, H., Botev, A., and Barber, D. Online structured Laplace approximations for overcoming catastrophic forgetting. In *Advances in Neural Information Processing Systems*, pp. 3738–3748, 2018. 2
- Rusu, A. A., Rabinowitz, N. C., Desjardins, G., Soyer, H., Kirkpatrick, J., Kavukcuoglu, K., Pascanu, R., and Hadsell, R. Progressive neural networks. *arXiv preprint arXiv:1606.04671*, 2016. 2
- Sato, M.-A. Online model selection based on the variational Bayes. *Neural computation*, 13(7):1649–1681, 2001. 2
- Schwarz, J., Czarnecki, W., Luketina, J., Grabska-Barwinska, A., Teh, Y. W., Pascanu, R., and Hadsell, R. Progress & compress: A scalable framework for continual learning. volume 80 of *Proceedings of Machine Learning Research*, pp. 4528–4537, 10–15 Jul 2018. 2
- Shi, J., Titsias, M. K., and Mnih, A. Sparse orthogonal variational inference for Gaussian processes. In *Artificial Intelligence and Statistics*, 2020. 5
- Shin, H., Lee, J. K., Kim, J., and Kim, J. Continual learning with deep generative replay. In *Advances in Neural Information Processing Systems*, pp. 2990–2999, 2017. 2
- Swaroop, S., Nguyen, C. V., Bui, T. D., and Turner, R. E. Improving and understanding variational continual learning. *arXiv:1905.02099 [cs, stat]*, 2019. 2, 5, 7, 8
- Thrun, S. Lifelong learning algorithms. In *Learning to learn*, pp. 181–209. Springer, 1998. 1
- Titsias, M. Variational learning of inducing variables in sparse Gaussian processes. In *Artificial Intelligence and Statistics*, pp. 567–574, 2009. 2, 3
- Titsias, M. K., Schwarz, J., Matthews, A. G. d. G., Pascanu, R., and Teh, Y. W. Functional regularisation for continual learning with Gaussian processes. In *International Conference on Learning Representations*, 2020. 2
- van de Ven, G. M. and Tolias, A. S. Three scenarios for continual learning. *arXiv preprint arXiv:1904.07734*, 2019. 2
- Wenzel, F., Roth, K., Veeling, B. S., Światkowski, J., Tran, L., Mandt, S., Snoek, J., Salimans, T., Jenatton, R., and Nowozin, S. How good is the Bayes posterior in deep neural networks really? *arXiv preprint arXiv:2002.02405*, 2020. 4
- Wilson, A. G. and Izmailov, P. Bayesian deep learning and a probabilistic perspective of generalization. *arXiv preprint arXiv:2002.08791*, 2020. 4
- Wilson, A. G., Hu, Z., Salakhutdinov, R., and Xing, E. P. Deep kernel learning. In *Artificial Intelligence and Statistics*, pp. 370–378, 2016. 13
- Zaheer, M., Reddi, S., Sachan, D., Kale, S., and Kumar, S. Adaptive methods for nonconvex optimization. In *Advances in Neural Information Processing Systems*, pp. 9793–9803, 2018. 6

Zenke, F., Poole, B., and Ganguli, S. Continual learning through synaptic intelligence. In *34th International Conference on Machine Learning*, pp. 3987–3995, 2017. 2, 6, 8

## A. VAR-GPs

### A.1. Posterior Predictive

For a novel input  $\mathbf{x}_*$ , the posterior predictive is computed via a Monte Carlo approximation of

$$p(y_* | \mathbf{x}_*) = \int p(y_* | f) q_t(f, \theta | \mathbf{x}_*) df d\theta \quad (12)$$

For a  $K$ -way classifier, we train  $K$  independent GPs and use the Bayes optimal prediction  $\arg \max_i p(y_*^{(i)} | \mathbf{x}_*)$ , for all  $i \in \{1, \dots, K\}$ , to compute accuracies.

## B. Ablations

### B.1. Global Inducing Points

This section outlines the assumptions made for the ablation titled as ‘‘Global’’. The characterization for the first task remains the same as in VAR-GPs. For subsequent tasks, the general model and the variational assumption is written as (with implicit dependence on  $\mathbf{Z}$ ),

$$\begin{aligned} p(\mathbf{y}^{(t)}, f, \theta | \mathbf{X}^{(t)}, \mathcal{D}^{(<t)}) &\approx \\ &\prod_{i=1}^{N_t} p(y_i^{(t)} | f, \mathbf{x}_i^{(t)}) \\ &p(f_{\neq \mathbf{u}_{t-1}} | \mathbf{X}^{(t)}, \mathbf{u}_{t-1}, \theta) \\ &q(\mathbf{u}_{t-1}) q_{t-1}(\theta). \end{aligned} \quad (13)$$

Note that we don’t have the auto-regressive characterization of VAR-GPs in the model anymore and instead have an approximate dependence through the variational posterior for the previous task. We further note that,

$$\begin{aligned} p(f_{\neq \mathbf{u}_{t-1}} | \mathbf{X}^{(t)}, \mathbf{u}_{t-1}, \theta) &= p(f_{\neq \mathbf{u}_{t-1}, \mathbf{u}_t} | \mathbf{X}^{(t)}, \mathbf{u}_{t-1}, \mathbf{u}_t, \theta) \\ &\frac{p(\mathbf{u}_{t-1}, \mathbf{u}_t | \theta)}{p(\mathbf{u}_{t-1} | \theta)}, \end{aligned} \quad (14)$$

$$\begin{aligned} p(f_{\neq \mathbf{u}_t} | \mathbf{X}^{(t)}, \mathbf{u}_t, \theta) &= p(f_{\neq \mathbf{u}_{t-1}, \mathbf{u}_t} | \mathbf{X}^{(t)}, \mathbf{u}_{t-1}, \mathbf{u}_t, \theta) \\ &\frac{p(\mathbf{u}_{t-1}, \mathbf{u}_t | \theta)}{p(\mathbf{u}_t | \theta)}. \end{aligned} \quad (15)$$

Owing to key cancellations, the variational lower bound now is given by,

$$\begin{aligned} \mathcal{F}(q_t) &= \sum_{i=1}^{N_t} \mathbb{E}_{q_t(f, \theta)} \left[ \log p \left( y_i^{(t)} | f, \mathbf{x}_i^{(t)} \right) \right] \\ &- \mathcal{KL} [q_t(\theta) || q_{t-1}(\theta)] \\ &- \mathbb{E}_{q_t(\theta)} [\mathcal{KL} [q(\mathbf{u}_t) || p(\mathbf{u}_t | \theta)]] \\ &+ \mathbb{E}_{q_t(\theta) q(\mathbf{u}_t | \theta) p(\mathbf{u}_{t-1} | \mathbf{u}_t, \theta)} \left[ \log \frac{q(\mathbf{u}_{t-1})}{p(\mathbf{u}_{t-1} | \theta)} \right]. \end{aligned} \quad (16)$$

A key difference to note here is that the  $\mathcal{KL}$  regularizer containing inducing points  $\mathbf{u}_t$  is not conditional on the previous ones anymore.

### B.2. Re-VAR-GP: Retraining old inducing points

In this version of VAR-GP, we allow retraining of old inducing points and call it Retractable VAR-GP (abbreviated as Re-VAR-GP). We clarify the precise nature of terms. Leading from (6) and (8), we highlight frozen  $\tilde{\mathbf{u}}_{<t}$  and  $\tilde{\mathbf{Z}}_{<t}$  (with a tilde) in the prior model to differentiate against learnable parameters,

$$\begin{aligned} p(\mathbf{y}^{(t)}, f, \theta | \mathbf{X}^{(t)}, \mathcal{D}^{(<t)}) &= \prod_{i=1}^{N_t} p(y_i^{(t)} | f, \mathbf{x}_i^{(t)}) \\ &p(f_{\neq \mathbf{u}_t, \tilde{\mathbf{u}}_{<t}} | \mathbf{X}^{(t)}, \mathbf{u}_t, \tilde{\mathbf{u}}_{<t}, \mathbf{Z}_t, \tilde{\mathbf{Z}}_{<t}, \theta) \\ &p(\mathbf{u}_t | \mathbf{Z}_t, \tilde{\mathbf{u}}_{<t}, \tilde{\mathbf{Z}}_{<t}, \theta) \\ &q(\tilde{\mathbf{u}}_{<t} | \tilde{\mathbf{Z}}_{<t}, \theta) q_{t-1}(\theta). \end{aligned} \quad (17)$$

We posit the variational posterior as,

$$\begin{aligned} q_t(f, \theta) &= p(f_{\neq \mathbf{u}_t, \mathbf{u}_{<t}} | \mathbf{X}^{(t)}, \mathbf{u}_t, \mathbf{u}_{<t}, \mathbf{Z}_t, \mathbf{Z}_{<t}, \theta) \\ &q(\mathbf{u}_t | \mathbf{Z}_t, \mathbf{u}_{<t}, \mathbf{Z}_{<t}, \theta) \\ &q(\mathbf{u}_{<t} | \mathbf{Z}_{<t}, \theta) q_t(\theta) \end{aligned} \quad (18)$$

To simplify these equations, we note the following identities.

$$\begin{aligned} p(f_{\neq \mathbf{u}_t, \mathbf{u}_{<t}} | \mathbf{X}^{(t)}, \mathbf{u}_t, \mathbf{u}_{<t}, \mathbf{Z}_t, \mathbf{Z}_{<t}, \theta) &= \\ p(f_{\neq \mathbf{u}_t, \mathbf{u}_{<t}, \tilde{\mathbf{u}}_{<t}} | \mathbf{X}^{(t)}, \mathbf{u}_t, \mathbf{u}_{<t}, \tilde{\mathbf{u}}_{<t}, \mathbf{Z}_t, \mathbf{Z}_{<t}, \tilde{\mathbf{Z}}_{<t}, \theta) \\ p(\tilde{\mathbf{u}}_{<t} | \mathbf{u}_t, \mathbf{u}_{<t}, \mathbf{Z}_t, \mathbf{Z}_{<t}, \tilde{\mathbf{Z}}_{<t}, \theta), \end{aligned}$$

$$\begin{aligned} p(f_{\neq \mathbf{u}_t, \tilde{\mathbf{u}}_{<t}} | \mathbf{X}^{(t)}, \mathbf{u}_t, \tilde{\mathbf{u}}_{<t}, \mathbf{Z}_t, \tilde{\mathbf{Z}}_{<t}, \theta) &= \\ p(f_{\neq \mathbf{u}_t, \mathbf{u}_{<t}, \tilde{\mathbf{u}}_{<t}} | \mathbf{X}^{(t)}, \mathbf{u}_t, \mathbf{u}_{<t}, \tilde{\mathbf{u}}_{<t}, \mathbf{Z}_t, \mathbf{Z}_{<t}, \tilde{\mathbf{Z}}_{<t}, \theta) \\ p(\mathbf{u}_{<t} | \mathbf{u}_t, \tilde{\mathbf{u}}_{<t}, \mathbf{Z}_t, \mathbf{Z}_{<t}, \tilde{\mathbf{Z}}_{<t}, \theta), \end{aligned}$$

$$\begin{aligned} &\frac{p(\mathbf{u}_t | \mathbf{Z}_t, \tilde{\mathbf{u}}_{<t}, \tilde{\mathbf{Z}}_{<t}, \theta) p(\mathbf{u}_{<t} | \mathbf{u}_t, \tilde{\mathbf{u}}_{<t}, \mathbf{Z}_t, \mathbf{Z}_{<t}, \tilde{\mathbf{Z}}_{<t}, \theta)}{p(\tilde{\mathbf{u}}_{<t} | \mathbf{u}_t, \mathbf{u}_{<t}, \mathbf{Z}_t, \mathbf{Z}_{<t}, \tilde{\mathbf{Z}}_{<t}, \theta)} \\ &= \frac{p(\mathbf{u}_{<t}, \mathbf{u}_t | \mathbf{Z}_t, \mathbf{Z}_{<t}, \theta)}{p(\tilde{\mathbf{u}}_{<t} | \tilde{\mathbf{Z}}_{<t}, \theta)}. \end{aligned}$$

Using these identities, the lower bound now simplifies as,

$$\begin{aligned} \mathcal{F}(q_t) &= \sum_{i=1}^{N_t} \mathbb{E}_{q_t(f, \theta)} \left[ \log p \left( y_i^{(t)} | f, \mathbf{x}_i^{(t)} \right) \right] \\ &- \mathcal{KL} [q_t(\theta) || q_{t-1}(\theta)] \\ &- \mathbb{E}_{q_t(\theta)} [\mathcal{KL} [q(\mathbf{u}_{\leq t} | \mathbf{Z}_{\leq t}, \theta) || p(\mathbf{u}_{\leq t} | \mathbf{Z}_{\leq t}, \theta)]] \\ &- \mathbb{E}_{q_t(\theta) q(\mathbf{u}_{\leq t} | \mathbf{Z}_{\leq t}, \theta) p(\tilde{\mathbf{u}}_{<t} | \tilde{\mathbf{Z}}_{<t}, \mathbf{u}_{\leq t}, \mathbf{Z}_{\leq t}, \theta)} [\mathcal{R}_t], \end{aligned} \quad (19)$$

where  $\mathfrak{R}_t = \log \frac{p(\tilde{\mathbf{u}}_{\leq t} | \tilde{\mathbf{Z}}_{\leq t}, \theta)}{q(\tilde{\mathbf{u}}_{\leq t} | \tilde{\mathbf{Z}}_{\leq t}, \theta)}$ . The key differences to note here are the fact that prior model now conditions on the frozen inducing points while the new variational distributions introduced are still free to optimize those points further. This leads to additional terms in the variational lower bound. We briefly discuss the performance next.

### B.2.1. PERFORMANCE ON TOY DATASET

Similar in spirit to Figure 1, we train Re-VAR-GP on the toy dataset in Figure 2. The density plots for training after both first task (training on classes 0/1) and the second (training on classes 2/3) are presented in Figure 7.

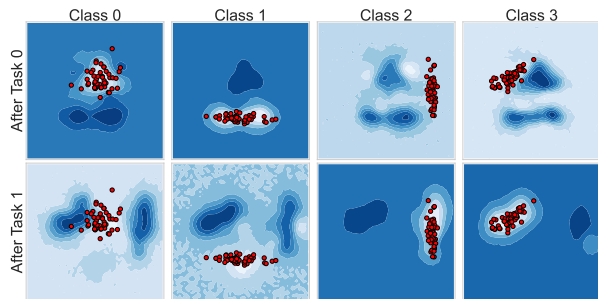


Figure 7. This figure shows class-wise output probabilities in each column for classifiers trained using a synthetic dataset (Figure 2) on the 2-D plane  $x, y \in [-3., 3.]$ . The first row represents the density surface after training for **Task 0** (observing classes 0/1) and the second after training for **Task 1** (observing classes 2/3). Brighter regions represent higher probabilities. Training points for each class are marked  $\bullet$ . Re-VAR-GP tends to suffer from catastrophic forgetting. Notice the approximately uniform uncertainty in regions for Class 0 and Class 1 after training on the second task.

As shown in Figure 7, Re-VAR-GP is not able to retain the information gained from previous task, a sign of catastrophic forgetting. This can be understood from the nature of the lower bound in (19). The only term that can potentially contribute to preservation of old information is the expected ratio  $\log \frac{p(\tilde{\mathbf{u}}_{\leq t} | \tilde{\mathbf{Z}}_{\leq t}, \theta)}{q(\tilde{\mathbf{u}}_{\leq t} | \tilde{\mathbf{Z}}_{\leq t}, \theta)}$ . However, this term avoids any interaction between  $\tilde{\mathbf{u}}_{\leq t}$  and  $\mathbf{u}_{\leq t}$ . As a result, the retrainable parameters  $\mathbf{u}_{\leq t}$  and  $\mathbf{Z}_{\leq t}$  have no information-preserving regularization unlike VAR-GPs as seen in (8). Owing to this observation, we do not pursue this model further.

### B.3. Deep Kernel Learning

For increased representational power in the kernel, we also provide preliminary experiments with Deep Kernel Learning (Wilson et al., 2016). Effectively, we augment the Exponentiated Quadratic kernel with a feature extractor  $g_\phi(x)$  in the form of a neural network and allow them to be trained

with additional kernel hyperparameters  $\phi$ . This amounts to replacing  $\mathbf{x}$  and  $\mathbf{x}'$  in (20) with  $g_\phi(\mathbf{x})$  and  $g_\phi(\mathbf{x}')$  respectively. We only use point estimates for  $\phi$ , initialized at the previous task for all  $t > 1$ .

#### B.3.1. EXPERIMENTS WITH SPLIT MNIST

We use a neural network with two hidden layers of size 256 each and the final output feature size of 64 to parameterize  $f_\phi$  and train the system end-to-end. As we see in Figure 8, the performance declines much faster than in VAR-GPs.

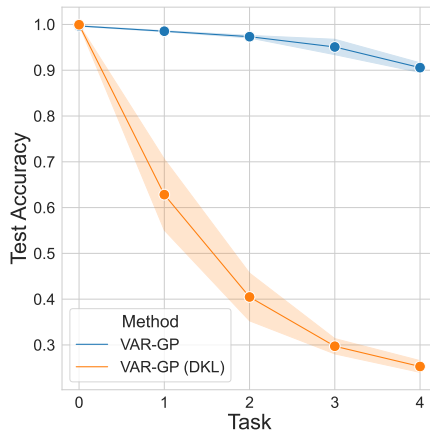


Figure 8. This figure shows the task-wise test accuracy on Split MNIST over five independent runs. We train a neural network as a feature extractor before applying the kernel (as described in Appendix B.3). It is clear that the neural networks require stronger regularization as we incorporate more tasks.

This result hints towards weak regularization of the feature extractor as we encounter subsequent tasks. The introduction of a neural network makes the inference problem much harder and any potential remedies are beyond the scope of current work. We, therefore, do not discuss this further but makes for an exciting direction to pursue in the future.

## C. Implementation

### C.1. Exponentiated Quadratic kernel

The precise parametrization of the kernel used is given below.  $\|\cdot\|_2$  is the  $\ell^2$ -norm. We parameterize  $\log \gamma$  and  $\log \sigma$ .

$$k(\mathbf{x}, \mathbf{x}') = \gamma \exp \left\{ -\frac{\|\mathbf{x} - \mathbf{x}'\|_2^2}{2\sigma^2} \right\} \quad (20)$$

### C.2. Parameterizing covariance matrices

In all experiments, we parameterize a covariance matrix  $\Sigma \in \mathbb{R}^{M \times M}$  using its Cholesky decomposition  $\Sigma = \mathbf{L}\mathbf{L}^\top$ , where  $\mathbf{L} \in \mathbb{R}^{M \times M}$  is a lower triangular matrix with positive diagonals. The positivity of the diagonals is maintained

via a `softplus` transform. As a result, we can apply unconstrained optimization on  $\frac{1}{2}(M \times (M + 1))$  free parameters corresponding to the lower triangular matrix  $\mathbf{L}$ .

### C.3. Computing the auto-regressive distributions in VAR-GPs

When using the auto-regressive parametrization in VAR-GPs, the joint distribution over all inducing points up to and including the current time step can be decomposed as follows,

$$\begin{aligned} q(\mathbf{u}_{\leq t}|\theta) &= q(\mathbf{u}_{< t}|\theta)q(\mathbf{u}_t|\mathbf{u}_{< t}, \theta) \\ &= \mathcal{N}(\mathbf{u}_{< t}; \mathbf{m}_{< t}, \boldsymbol{\Sigma}_{< t}) \\ &\quad \mathcal{N}(\mathbf{u}_t; \mathbf{A}_t\mathbf{u}_{< t} + \mathbf{m}_t, \boldsymbol{\Sigma}_t), \end{aligned} \quad (21)$$

such that  $\mathbf{A}_t = \mathbf{K}_{\mathbf{z}_t, \mathbf{z}_{< t}} \mathbf{K}_{\mathbf{z}_{< t}, \mathbf{z}_{< t}}^{-1}$ .

While we cannot avoid sampling the hyperparameters  $\theta$ , we can avoid variance introduced by the ancestral sampling of variational distribution for computation of (8). We recognize that the full auto-regressive distribution can be computed in closed form as it is a product Gaussians with linear dependence in the mean, similar in spirit to linear Gaussian dynamical systems (Murphy, 2012). Hence, for all  $t > 1$ , we have

$$q(\mathbf{u}_{\leq t}|\theta) = \mathcal{N}\left(\begin{bmatrix} \mathbf{u}_{< t} \\ \mathbf{u}_t \end{bmatrix}; \begin{bmatrix} \mathbf{m}_{< t} \\ \mathbf{A}_t\mathbf{m}_{< t} + \mathbf{m}_t \end{bmatrix}, \boldsymbol{\Sigma}\right) \quad (22)$$

where,

$$\boldsymbol{\Sigma} \triangleq \begin{bmatrix} \boldsymbol{\Sigma}_{< t} & \boldsymbol{\Sigma}_{< t}\mathbf{A}_t^\top \\ \mathbf{A}_t\boldsymbol{\Sigma}_{< t}^\top & \boldsymbol{\Sigma}_t + \mathbf{A}_t\boldsymbol{\Sigma}_{< t}\mathbf{A}_t^\top \end{bmatrix}$$

## D. Hyperparameters

### D.1. Search Space

The search space for all hyperparameters used across experiments is described in Table 2. Top hyperparameters were picked using a held-out validation set.

Table 2. List of key hyperparameters with relevant search spaces.

Hyperparameter	Range / Value
Learning Rate ( $\eta$ )	[0.001, 0.01]
Inducing Points ( $M$ )	[40, 200]
Hypers $\mathcal{KL}$ Tempering Factor ( $\beta$ )	[1.0, 10.0]
Batch Size (B)	512
Maximum Epochs (E)	500
Early Stopping Patience Epochs (K)	200
Early Stopping Tolerance ( $\delta$ )	0.0001

### D.2. Varying number of inducing points $M$

In Figure 9, we note the mean performance by varying the number of inducing points  $M$  from 20 to 200 in steps of 20, for Split MNIST. The key takeaway here is that increasing the number of inducing points generally does improve the performance. This indicates that there may be more capacity available to be exploited further.

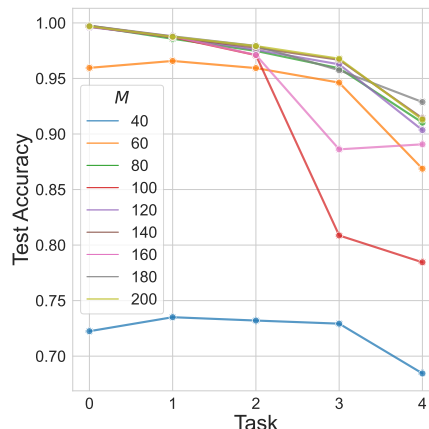


Figure 9. This figure shows the mean task-wise (on x-axis) test accuracy (y-axis) on Split MNIST over five independent runs, varying number of inducing points  $M$  from 20 to 200 in steps of 20. The key insight to draw here is about the general trend that increasing the number of inducing points  $M$  improves the mean performance, hinting towards more capacity being available to be exploited by the learning algorithm.